



Hydrothermal synthesized zinc oxide/kaolinite for photo-decolorization of methyl violet

Is Fatimah*, Rico Nurillahi, Fitriana Harjanti

Chemistry Department, Universitas Islam Indonesia, Kampus Terpadu UIII, Jl. Kaliurang Km 14, Sleman, Yogyakarta, Indonesia, emails: isfatimah@uii.ac.id (I. Fatimah), riconurillahi@uii.ac.id (R. Nurillahi), fitrianaaharjanti@uii.ac.id (F. Harjanti)

Received 26 July 2019; Accepted 13 December 2019

ABSTRACT

A composite of zinc oxide supported on kaolinite (ZnO/Kao) using Indonesian natural kaolinite minerals was synthesized by a hydrothermal method. The role of the material as a photocatalyst in methyl violet (MV) photocatalytic decolorization was tested. As-prepared material was characterized by X-ray diffraction, scanning electron microscope analysis, transmission electron microscope analysis, and diffuse reflectance UV-Vis diffuse reflectance spectroscopy. The results showed that significant photocatalytic activity for the photocatalytic decolorization of MV was found compared to ZnO. The increased photocatalytic activity was related to the band gap energy associated with the formation of nanoparticles (crystallite size of 46–74 nm). In addition, the material demonstrated high decolorization efficiency as measured by a turnover number (TON) and photocatalyst stability at varied pH ranges from 4–10. The results suggest that the material may be a promising photocatalyst for photocatalytic decolorization of organic dyes in wastewater.

Keywords: Dye degradation; Photo-decolorization; ZnO/Kaolinite; Kaolinite

1. Introduction

Dyes containing wastewater are produced by many industries, such as textiles, printing, paper, and leather. According to current estimates, approximately 7×10^5 tons of dyes are produced annually [1]. These dyes require treatment before they are discharged into the environment. The majority of compounds used in dyes has carcinogenic properties and therefore are harmful both to humans and the aquatic environment [2,3]. Various chemical and physicochemical treatments have been developed to address dye-related pollution [2]. Among these, photocatalysis has attracted much attention, as it offers many benefits as compared with those of other techniques, such as adsorption, ozonization, and chemical oxidation. For example, unlike adsorption, photocatalysis produces no by-products that require further treatment. It is also less costly than ozonization and chemical oxidation treatments [4,5].

Many photocatalysts, such as TiO_2 , ZnO, Fe_2O_3 , and ZrO_2 , have been applied in dye degradation [6,7]. Among these, ZnO is preferable due to its wide band gap energy and stability [8,9]. However, to be suitable for use at the industrial scale, where reusability affects the costs of dye degradation, the photocatalytic activity and stability of ZnO need to be enhanced. Various modifications, such as doping, composite formation, and immobilization of photocatalytic active material in solid support, have been proposed [10–12]. The use of a supporting metal oxide photocatalyst in solid support was reported to be stable and low-cost solids were reported to be effective by the contributing adsorption capability from the support for the photocatalytic mechanism.

Several studies reported ZnO immobilization using zeolite [13], SiO_2 [14], and bentonite [15]. Among solids, clay minerals have particular properties that are useful for improving photocatalytic activity [16,17]. The present study

* Corresponding author.

examined the physicochemical properties and photocatalyst performance of ZnO immobilized in a clay material, kaolinite, to form a composite of ZnO/kaolinite (ZnO/Kao). Although the preparation of this composite has been described in the past, to our knowledge, there have been no studies on its use in methyl violet (MV) decolorization. Another novel aspect of the present study was the use of natural kaolinite from Indonesia.

2. Materials and methods

2.1. Materials

Kaolinite was obtained from Sukabumi, West Java, Indonesia. Chemicals consist of MV, zinc acetate dihydrate, sodium hydroxide, and ethanol was purchased from Merck-Millipore (Germany). All the chemicals were of analytical grade and were used without further purification.

2.2. Material preparation

ZnO supported on kaolinite (ZnO/Kao) was prepared by mixing a precursor solution composed of a mixture of zinc acetate and sodium hydroxide solution at a molar ratio of Zn:OH = 2:1 with a kaolinite suspension (20% wt.). The ZnO/Kao composites were varied at varied Zn content so the ZnO weight percentage were 10%, 30%, and 50% wt. The mixture was placed in an autoclave and kept at 150°C overnight. The resulting solid phase was filtered and washed using distilled water until the conductivity of the filtrate was less than 100 mS/cm. The solid was then dried at 105°C and calcined at 400°C for 4 h. The prepared materials were encoded as ZnO/Kao-10, ZnO/Kao-30 and ZnO/Kao-50, respectively. For comparison purposes, bulk ZnO was also synthesized using a method reported previously [18].

Physicochemical characterization of the materials was conducted by X-ray diffraction (XRD), gas sorption analysis, scanning electron microscope-energy-dispersive X-ray analysis (SEM-EDX), transmission electron microscope analysis, and UV-Vis diffuse reflectance spectroscopy (UV-DRS). The XRD patterns were recorded in the Rigaku diffractometer mode under Ni-filtered CuK α irradiation ($\lambda = 1.7889 \text{ \AA}$). The specific surface area, pore-volume, and pore radius of the materials were calculated based on adsorption-desorption isotherm analysis using a NOVA 1200e instrument (Tokyo, Japan). The pore size distribution in the desorption profile was evaluated using the Barrett-Joyner-Halenda (BJH) equation. A JASCO V760 spectrophotometer was utilized for the UV-DRS measurements. The band gap energy was determined using the Kubelka-Munk function as the intercept from the plot of $(F(R_{\infty})/hv)^{1/2}$ vs. hv based on the following Eq. (1):

$$F(R_{\infty}) = \frac{(1 - R_{\infty})^2}{2R_{\infty}}, \quad (1)$$

where R_{∞} was the measured absolute reflectance of the sample ($R_{\text{sample}}/R_{\text{standard}}$).

The spectrum at 190–850 nm was obtained, using BaSO₄ powder as reference material.

The morphology and elemental composition of the samples were observed using an SEM (JEOL) with an accelerating voltage of 5 kV. The photocatalytic activity of the materials in terms of MV decolorization was evaluated in a batch reactor. The UV light was provided by a 30 W UV lamp with a wavelength of 296 nm. The mixture of the MV solution and photocatalyst was magnetically stirred in the dark for 15 min prior to light exposure. For the quantitative analysis of MV, its absorption spectrum was measured using a V-Vis HITACHI U-2010 spectrophotometer.

To compare the photocatalytic activity of the catalysts at an equivalent amount of ZnO, the decolorization efficiency (DE) and turnover frequency (TON) were measured using the following Eqs. (2) and (3):

$$DE = \frac{C_0 - C_t}{C_0} \times 100 \quad (2)$$

$$\text{TON} (\% / \text{mg ZnO}) = \frac{DE}{(m_{\text{cat}} \times t)} \quad (3)$$

with C_0 and C_t is an initial concentration of MV and the concentration at time t , m_{cat} is mass of photocatalyst, and t is a time of measurement (60 min).

3. Results and discussion

3.1. Physicochemical character of ZnO/Kao

The XRD patterns of ZnO/Kao at varied ZnO content and its comparison with those of kaolinite and bulk ZnO are depicted in Fig. 1. The XRD pattern of the kaolinite sample shows reflections specific for kaolinite that fit those of the JCPD standard (PDF-01-089-6538), with some reflections indicative of the presence of quartz. The composite formation of ZnO/Kao exhibited a combination of a wurtzite phase of ZnO reflections (JCPDS No. 36-1451) and kaolinite.

The reflections were identified at $2\theta = 31.67^\circ$, 34.31° , 36.14° , 47.40° , 56.52° , and 62.73° , which are associated with (1 0 0), (0 0 2), (1 0 1), (1 0 2), (1 1 0), and (1 0 3) [19]. The crystallite size of ZnO in the composites was determined using Scherrer's Eq. (4):

$$D_p = \frac{0.94\lambda}{\beta \cos\theta} \quad (4)$$

where D_p was the size of the crystallites b was the line broadening in radians, q was the reflection angle, and l was the X-ray wavelength. From varied ZnO content, the calculated crystallite size was 46, 68, and 74 nm, respectively (Table 1).

The presence of ZnO in the composite was revealed by a change in the surface profile, as indicated by SEM morphology (Fig. 2), and elemental analysis results from SEM-EDX analysis (Table 2). The transmission electron microscope analysis of ZnO/Kao-30 revealed irregular and heterogeneous ZnO nanoparticles with sizes ranging from 40 to 80 nm (Fig. 2b).

The kaolinite surface morphology exhibited a flake-like appearance, similar to that of kaolinite reported in previous studies. After modification with ZnO, a flower-like

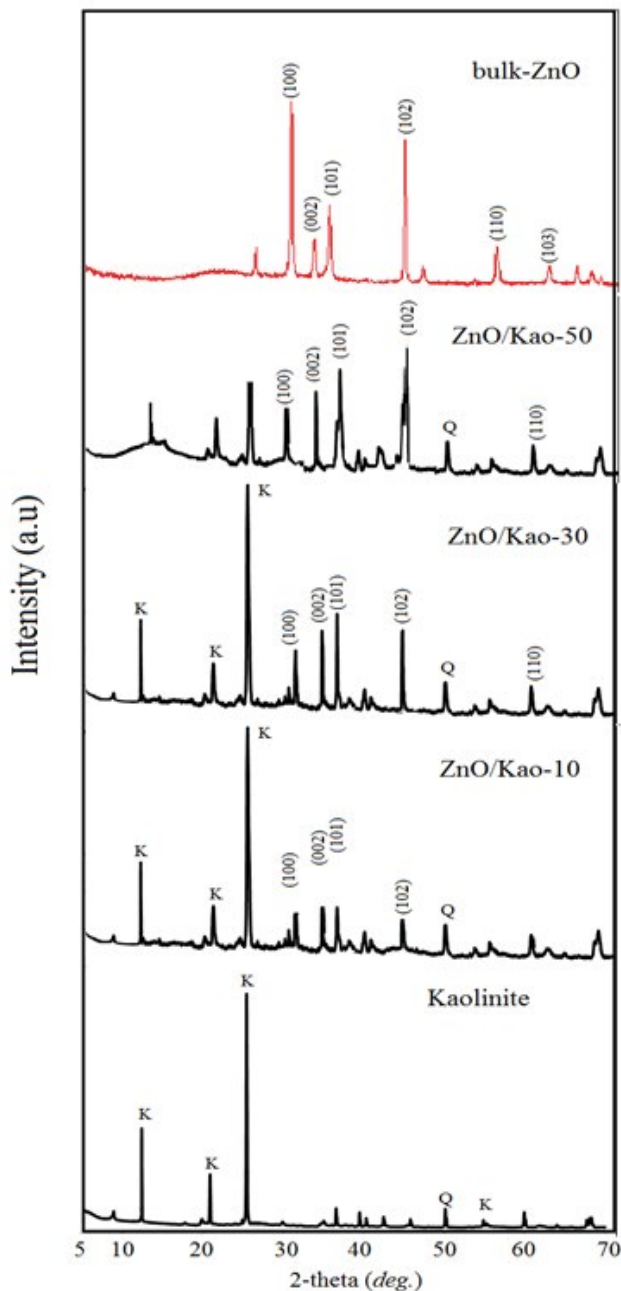


Fig. 1. XRD pattern of ZnO/Kao samples in comparison with kaolinite and bulk-ZnO.

Table 1
Surface profile parameters of kaolinite, ZnO/Kao and bulk-ZnO

Sample	BET specific surface area (m ² /g)	Pore volume (cc/g)	Pore radius (Å)	ZnO crystallite size (nm)
Kaolinite	15.46	2.85 × 10 ⁻³	18.5	–
ZnO/Kao-10	18.39	3.82 × 10 ⁻³	9.78	46
ZnO/Kao-30	28.56	5.42 × 10 ⁻³	10.20	68
ZnO/Kao-50	22.67	4.56 × 10 ⁻³	11.45	74
Bulk-ZnO	26.45	8.66 × 10 ⁻³	17.56	76

formation was appeared on the surface, and the pattern is clearer as increasing ZnO content. The surface profile of ZnO/Kao was similar to that of previous research on ZnO/Kao, with a ZnO content ranging from 9.4% to 49.2% wt. (Table 1) [20]. The EDX spectra revealed that the main components of kaolinite were SiO₂ and Al₂O₃, and the ZnO contents in the ZnO/Kao10, ZnO/Kao-30 and ZnO/Kao-50 samples are 12.33%, 38.7%, and 49.67% wt, respectively. The chemical interaction between Zn and Si in the composite form is identified from the Fourier-transform infrared (FTIR) spectra presented in Fig. 3.

The characteristic peaks at 830 cm⁻¹ is appeared in both kaolinite and ZnO/Kao-30 samples indicating the presence of Si asymmetric and symmetric stretching, which indicate the presence of SiO₂. This peak is also strengthened by the peak for Si–O–Si bending at 1,514 cm⁻¹ and Si–OH at 1,386 cm⁻¹. The presence of ZnO is characterized by the peak at 738 and 642 cm⁻¹ for identify of Zn–O, and the absorption peak at 940 cm⁻¹ that corresponds to Si–O–Zn stretching [21,22].

The specific surface areas of the samples determined by the Brunauer–Emmett–Teller (BET) method (BET-specific surface area), as well as pore volume and pore radius determined by the BJH method, are listed in Table 1 based on the adsorption-desorption isotherm profile (Fig. 4). In general, it can be concluded that the BET-specific surface area of ZnO/Kao samples was higher than that of kaolinite and slightly higher than that of bulk-ZnO. By varying the ZnO content, it is seen that BET specific surface of materials is in the following order: ZnO/Kao-30 > ZnO/Kao-50 > ZnO/Kao-10. This finding was in agreement with the surface morphology results, pointing to the formation of the rougher surface in ZnO/Kao-30 and ZnO/Kao-50 compared with ZnO/Kao-10. The rougher surface represents the higher surface area providing more adsorption sites on the surface of the photocatalyst. The evolution of the parameters can be indicated from the pore distribution profile presenting a hysteresis loop, which confirmed the change of dominant pores from micropores into a combination of mesoporous and microporous range.

The capability of UV–Vis light absorption is an important property of a photocatalyst. In addition, the calculation of the band gap energy based on the absorption spectra is useful to identify the effective energy of photons in the photocatalysis mechanism. As shown in Fig. 5, the observed UV–Vis absorption spectra of the samples revealed a broad absorption band of ZnO/Kaos from the ultraviolet to the visible region, with the maximum absorption peaks found

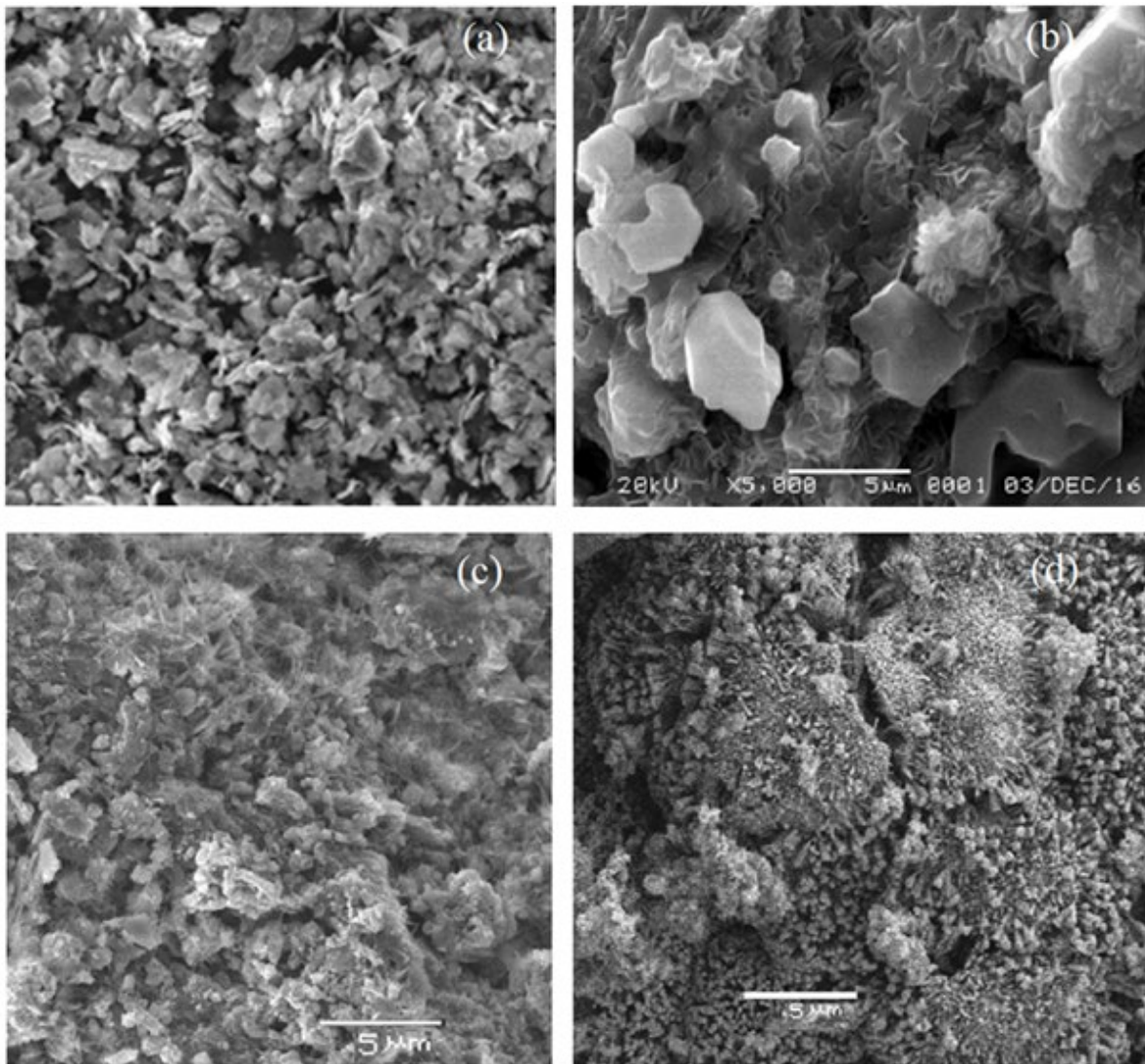


Fig. 2. SEM-EDX profile of (a) kaolinite, (b) ZnO/Kao-10, and (c) ZnO/Kao-30 ZnO/Kao-50.

Table 2
Elemental analysis results of materials

Compound (% wt.)	Kaolinite	ZnO/Kao-10	ZnO/Kao-30	ZnO/Kao-50	ZnO
Na ₂ O	0.13	0.13	0.12	0.08	–
MgO	0.60	0.61	0.43	0.19	–
Al ₂ O ₃	25.71	15.65	12.22	9.02	–
SiO ₂	66.56	65.23	42.74	35.1	0.06
CaO	0.27	0.2	0.17	0.07	–
K ₂ O	6.72	6.04	6.43	4.22	–
ZnO	nd	12.33	38.12	51.32	99.04

around 220–330 nm. ZnO/Kao showed higher absorption intensity in the UV region and visible region, and both had a similar edge wavelength at around 399–403 nm. The important point from the varying ZnO content is that the band spectrum is not significantly different in either the pattern

or the edge wavelength value. The calculation based on the Kubelka–Munk equation represented the plot of ZnO/Kao and bulk-ZnO with their corresponding band gap values of 3.18 and 3.22 eV, respectively. The obtained band gap energy of ZnO was similar to that of synthesized ZnO using rice

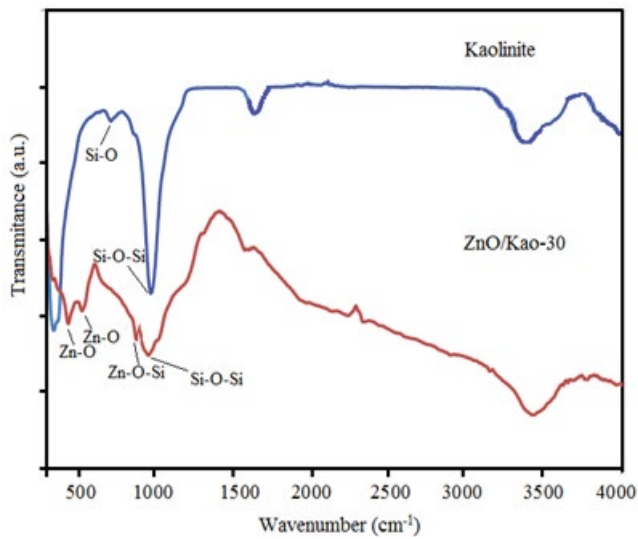


Fig. 3. Comparison of FTIR spectra of kaolinite and ZnO/Kao-30.

bran as a templating agent [23]. The higher band gap energy of ZnO/Kao as compared with that of ZnO was related to the crystallite size of ZnO in the nanosize range. A previous study reported that the band gap of semiconductor nanocrystals increased in accordance with a decrease in particle size [24]. Another study reports a similar phenomenon in a ZnO/zeolite composite [25].

3.2. Photocatalytic activity of ZnO/Kao

Fig. 6 shows the changes in the absorption spectra of the initial and treated MV solutions. As can be seen, the absorbance of the maxima wavelength decreased in accordance with an increase in the treatment time, with a shift in the maxima wavelength to a lower wavelength. Moreover, a peak at around 200–300 nm, which was associated with an aromatic structure of MV, disappeared in the treated solution.

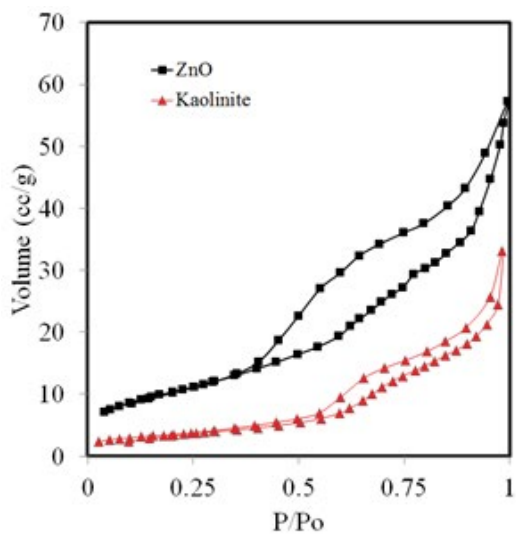


Fig. 4. Adsorption–desorption profile of materials.

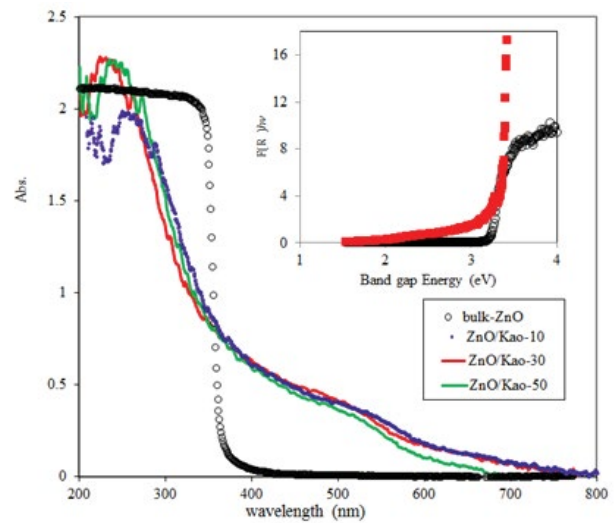
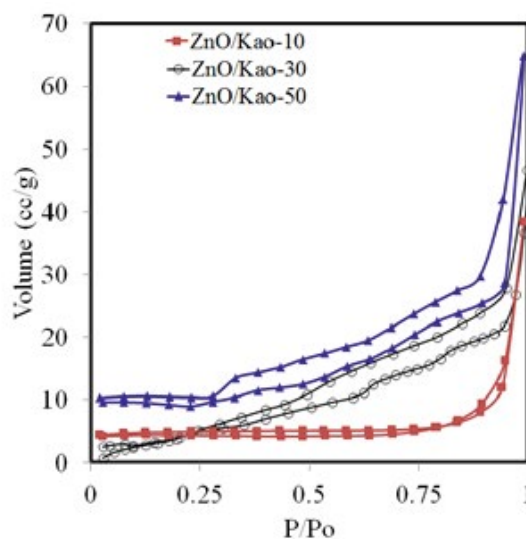


Fig. 5. DRUV spectra of ZnO/Kao samples and bulk-ZnO.

This observation confirmed that decolorization was the result of azo bond ($-N=N-$) destruction, as reported in other studies [26,27]. High-performance liquid chromatography (HPLC) analysis of the treated solutions revealed that decolorization was the result of not only an adsorption mechanism towards the dye molecules but also an oxidation mechanism as the degradation products identified and a smaller amount of oxidized organic compounds produced.

3.3. Effect of ZnO content to photocatalytic-decolorization of MV degradation

The kinetics of photo-decolorization and adsorption based on a colorimetric analysis of the various ZnO/Kao photocatalyst are presented in Fig. 7. It is seen that MV degradation by photocatalytic mechanism is faster compared with adsorption, suggesting that the photocatalysts are actively



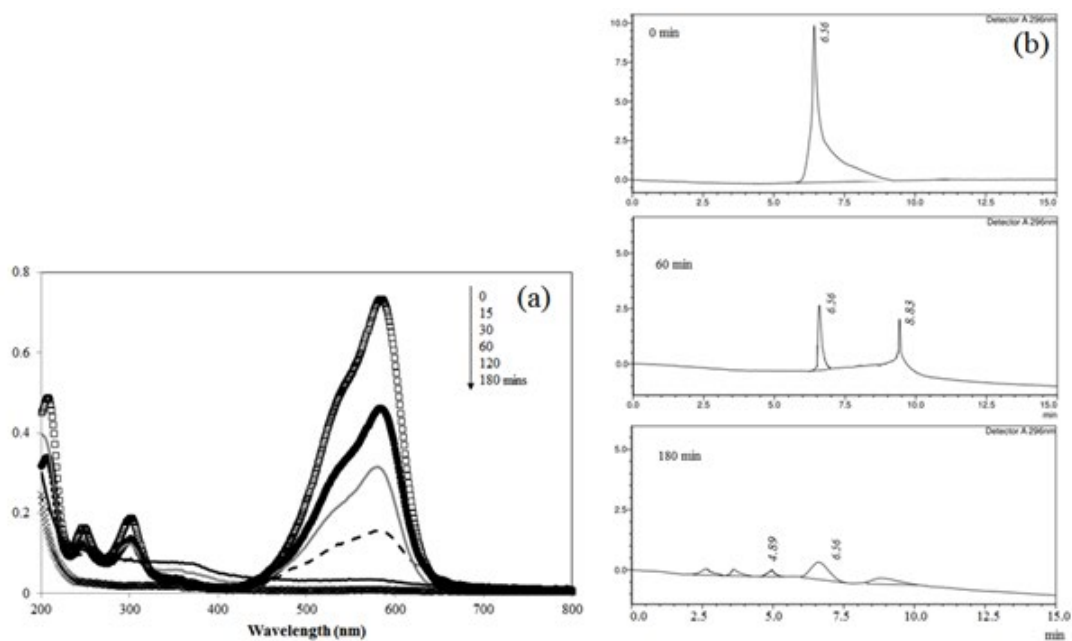


Fig. 6. (a) Changes in the absorption spectra of the initial and treated MV solutions and (b) chromatogram of initial and treated solution.

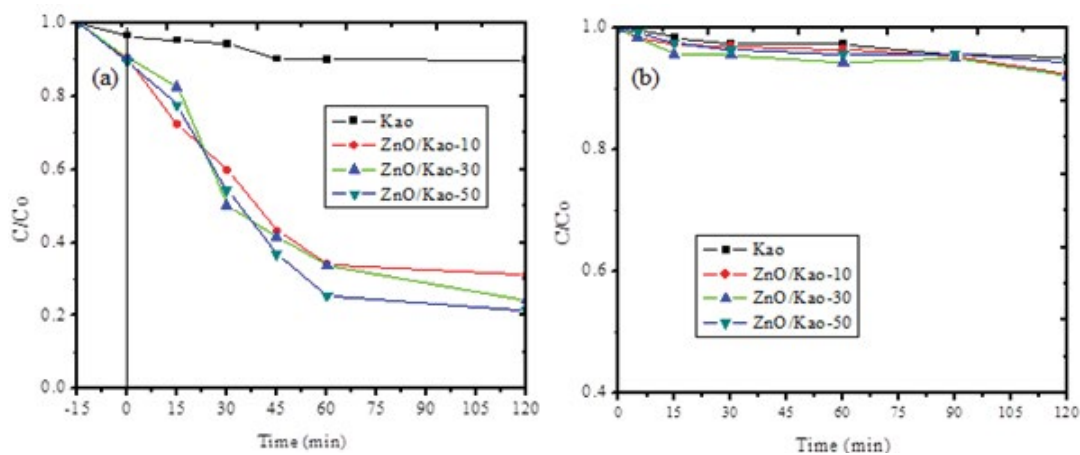


Fig. 7. (a) Kinetics of MV photo-decolorization using materials and (b) kinetics of MV adsorption using materials.

proven. The kinetics of photocatalytic-decolorization during the interval of 0–30 min seems not as influenced by different ZnO content, but then along with increasing time of treatment, the DEs are in the order ZnO/Kao-30 > ZnO/Kao-50 > ZnO/Kao-10. The order suggests that the photocatalytic activity is corresponding with the order of the BET-specific surface area of the photocatalyst.

3.4. Effect of MV initial concentration

Furthermore, in order to evaluate the mechanism of MV photo-decolorization, the kinetics of photo-decolorization and adsorption at the various MV initial concentrations by ZnO/Kao-30 photocatalyst were studied, and the kinetics plot is listed in Fig. 8. The significant difference in the

decolorization among photocatalytic decolorization compared with adsorption implies an identified photocatalytic activity of the material. From Fig. 8a, the calculation from the kinetics data suggest that all photo-decolorizations data fits with pseudo-second-order kinetics with the following Eq. (5):

$$\frac{1}{C_t} = kt + \frac{1}{C_0} \tag{5}$$

with C_0 and C_t are initial MV concentration and MV concentration at a time of t , and k is kinetics constant.

The photo-decolorization efficiencies decreased in accordance with an increase in the initial MV concentration from 40%–90% over a period of 60 min. The lower

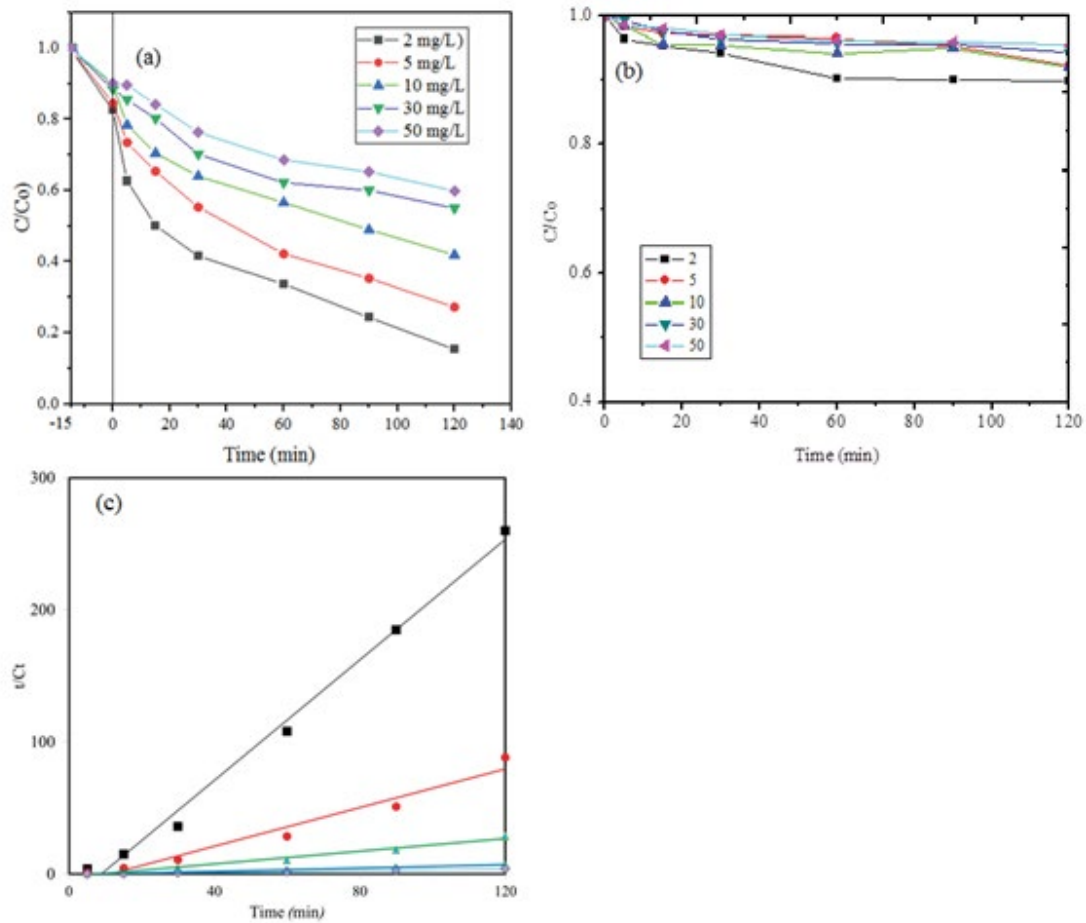


Fig. 8. (a) Kinetics of MV photo-decolorization is using ZnO/Kao-30 at varied initial concentration, (b) kinetics of MV adsorption using ZnO/Kao-30 at varied initial concentration, and (c) pseudo-second-order plot of MV photo-decolorization using ZnO/Kao-30.

concentration resulted in inefficient interactions among the molecules and their surface interactions for further oxidation mechanism. At a DE value of about 85% for an initial MV concentration of 2 mg/L after 60 min of treatment, the photocatalytic activity of ZnO/Kao was comparable to that of ZnO NPs prepared by precipitation of zinc acetate [28] and activated carbon-supported Bi-doped ZnO nanocomposite material (AC-Bi/ZnO) [29]. However, the photocatalytic activity of ZnO/Kao was significantly higher than that of ZnO nanorods, which had a DE value of only 56% [30]. Photocatalytic activity of ZnO/Kao in this research in comparison with various photocatalysts for MV photo-decolorization are listed in Table 3 shows that ZnO/Kao samples prepared in this research are comparable at the high activity as shown by DE higher than 80%.

Based on kinetics constant k from all varied MV concentration and ZnO/Kao photocatalysts, the Langmuir-Hinshelwood model was applied to study the effect of the initial concentration of MV on the rate of photo-decolorization which referred to following Eq. (6):

$$-\frac{dC}{dt} = k_r \theta = k C_e = \frac{k_r K_{LH} C_e}{1 + K_{LH} C_e} \quad (6)$$

Which was modified as:

$$\frac{1}{k} = \frac{1}{k_r k_{LH}} + \frac{1}{k_r} C_e \quad (7)$$

where θ denoted the surface coverage, k is the apparent kinetics constant, C_e was the concentration of BPB at adsorption equilibrium, and k_{LH} was the Langmuir-Hinshelwood adsorption constant. k_{L-H} was the adsorption-desorption kinetics equilibrium, and k_r represented the limiting rate of the reaction at maximum coverage under the given experimental conditions.

The Langmuir-Hinshelwood plot is presented in Fig. 9, and the parameters are listed in Table 4. According to the calculation, k_r and k_{LH} from all varied photocatalysts represent the higher k_r compared to k_{LH} points which are an indication that the reaction is not dominantly influenced by the adsorption mechanism. The capability of ZnO/Kao to catch the photon and produce oxidants for the degradation of the organic compound was effectively influenced by the presence of ZnO as a photoactive component in the mechanism [31,32]. It is confirmed by increasing k_r along with increasing ZnO content in the photocatalysts, and in reverse order, decreasing k_{LH} with increasing ZnO content.

The effect of the initial MV concentration on TON using ZnO/Kao-30 and bulk ZnO are depicted in Fig. 10. In comparison with the photocatalytic activity of bulk ZnO, the TON values of the reaction using ZnO/Kao-30 were higher than those of bulk ZnO. The TON values at varying initial MV concentrations were determined based on a photoactive

semiconductor, ZnO content in ZnO/Kao-30 (38.12% wt.) compared with 100% wt. for bulk ZnO. These higher values represented the more effective photocatalysis sites in the composite form. As the BET-specific surface areas of ZnO and ZnO/Kao-30 were not significantly different, the elevated TON was due to the increased capability of ZnO/

Table 3
Comparison of various photocatalysts for MV photo-decolorization

Photocatalyst	Degradation efficiency (%)	Remark	Reference
TiSiW ₁₂ O ₄₀ /TiO ₂	82.4	DE was evaluated for MV 20 mg ppm for 3 h of treatment	[31]
TiO ₂ /Pd	95	Time of degradation 20 min	[31]
TiO ₂ /Pt	78	Time of degradation 20 min	[31]
TiO ₂	97	Optimum dosage of photocatalyst of 0.15 g/100 cm ³	[32]
Composite of activated carbon-Bismuth-ZnO (AC-Bi/ZnO)	94.5	Irradiation time 60 min	[29]
H ₃ PW ₆ Mo ₆ O ₄₀ /SiO ₂	88.7	Treatment for 2.5 h for MV 10 ppm	[33]
ZnO-Kao-30	85	Treatment for 60 min, MV 2 ppm	This research

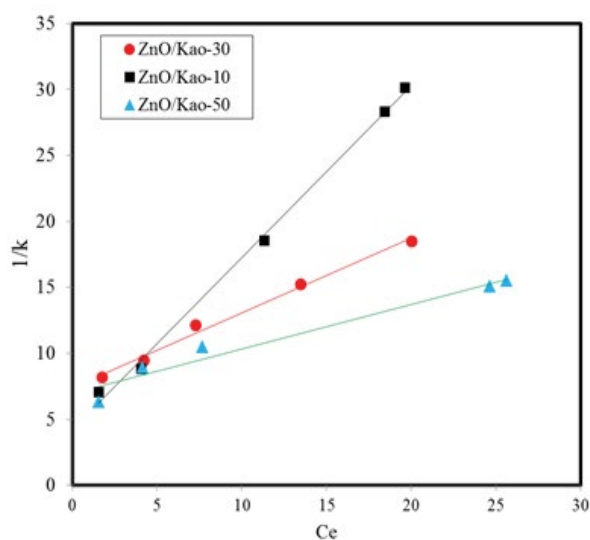


Fig. 9. Langmuir–Hinshelwood plot of MV photo-decolorization by using varied Zn/Kao samples.

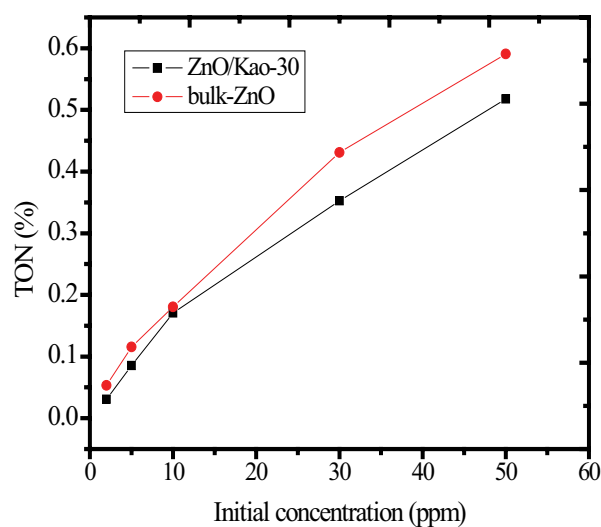


Fig. 10. Comparison of TON of MV photo-decolorization at varied initial concentrations using bulk-ZnO and ZnO/Kao-30.

Table 4
Parameters of Langmuir–Hinshelwood plot of photo-decolorization using varied ZnO/Kao

Photocatalyst	DE at 60 min (%)	Langmuir–Hinshelwood equation	R ²	k _r (mg/L min)	k _{LH} (L min/mg)
ZnO/Kao-10	65.90	$\frac{1}{k_{app}} = 4.20 + 1.30 \frac{1}{C_e}$	0.9984	0.77	0.31
ZnO/Kao-30	66.30	$\frac{1}{k_{app}} = 7.56 + 0.57 \frac{1}{C_e}$	0.9957	1.77	0.08
ZnO/Kao-30	74.60	$\frac{1}{k_{app}} = 6.95 + 0.38 \frac{1}{C_e}$	0.9800	2.97	0.05

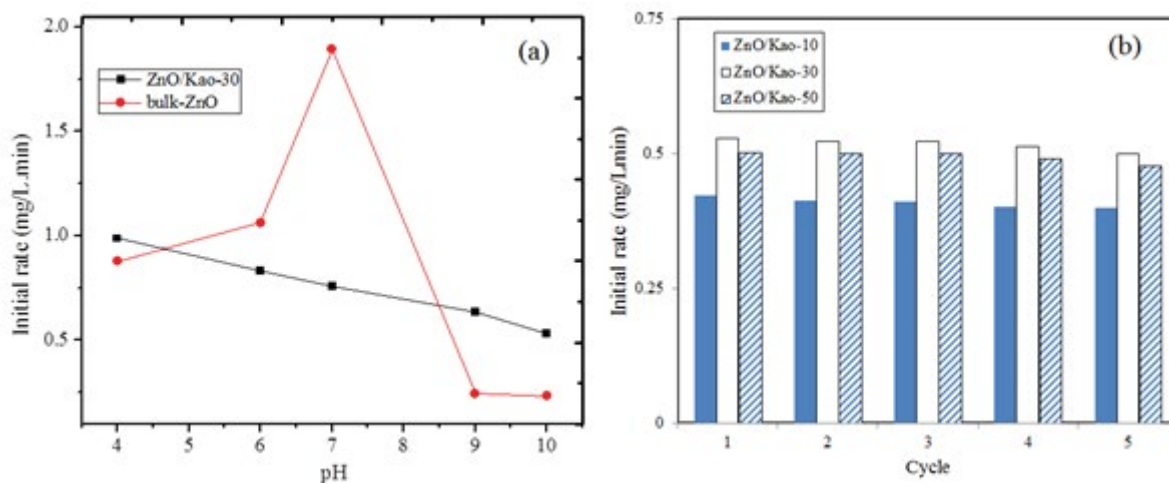


Fig. 11. Effect of the pH on the initial rate of photocatalytic decolorization using ZnO/Kao and bulk ZnO.

Kao-30 to adsorb light, which was also related to the nano-sized ZnO. Similar TON values were found for AC-Bi/ZnO containing 39% wt. of ZnO. The DE and TON values implied that ZnO/Kao-30 represented an effective photocatalyst for further applications in dye-containing wastewater treatment.

3.5. Effect of MV initial concentration

Considering that in applications a solution may have different pH conditions, the effect of pH on the photocatalytic activity was performed. Besides of this, reusability is another important aspect of applicability. Fig. 11 depicts the effect of the pH and use cycles on the initial rate of photo-decolorization. The effect of pH on the initial rate was studied by comparing the use of ZnO/Kao-30 and bulk ZnO. As shown in the plot, although the photocatalytic decolorization rate using ZnO/Kao consistently decreased along with an increase in the pH, the initial rate of the reaction remained stable at the tested pH ranges (4–10). The photocatalytic decolorization performance using bulk ZnO was best at pH = 7 and lost at basic pH conditions. These data suggested that the stability of ZnO/Kao was higher than that of bulk ZnO. The presence of kaolinite as support for ZnO stabilized the surface interaction between the dyes, as reported previously for photocatalytic decolorization of other dyes using clay-supported ZnO or silica-supported ZnO [34,35].

Moreover, the reusability study (Fig. 11b) demonstrates that all ZnO/Kao composites have stable photoactivity until 5 cycles as expressed by a relative unchanged initial rate for all varied ZnO/Kao samples. The pattern is similar to the stability of ZnO/kaolinite reported for photodegradation of 2-chlorophenol [36].

4. Conclusion

Composites of ZnO-immobilized on kaolinite were successfully synthesized using a hydrothermal method, and its photocatalytic activity in MV photocatalytic decolorization was studied. The ZnO/Kao composite material exhibited the formation of ZnO in the wurtzite phase deposited on kaolinite

ranging at 46–74 nm in crystallite size. The band gap energy values of the composites are lay at around 3.22 eV. The photocatalytic study of ZnO/Kao samples revealed that DE for initial MV of 2–50 ppm is at around 30%–95%. The advantages of composite formation are reflected by a higher turnover number of the photo-decolorization process by ZnO/Kao samples respect to the use of bulk ZnO, and higher stability at varied pH (4–10). The kinetics of the photo-decolorization process by using ZnO/Kao was found to obey pseudo-second-order kinetics and fit with the Langmuir–Hinshelwood mechanism.

References

- [1] D.A. Yaseen, M. Scholz, Textile dye wastewater characteristics and constituents of synthetic effluents: a critical review, *Int. J. Environ. Sci. Technol.*, 16 (2019) 1193–1226.
- [2] X.Q. Wang, F.P. Wang, X.H. Zeng, Q. Zhang, W. Zhang, J.Y. Le, S.Z. Yang, Decolorization of methyl violet in simulated wastewater by dielectric barrier discharge plasma, *Jpn. J. Appl. Phys.*, 54 (2015) 056201–056208.
- [3] A. Pirkarami, M.E. Olya, Removal of dye from industrial wastewater with an emphasis on improving economic efficiency and degradation mechanism, *J. Saudi Chem. Soc.*, 21 (2017) S179–S186.
- [4] J. Nugraha, I. Fatimah, Modeling of photocatalytic activity of ZnO/AC by using linear probability model, logit and complementary log transformation, *Procedia Eng.*, 148 (2016) 1112–1120.
- [5] S. Bagheri, A. Termehousefi, T.O. Do, Photocatalytic pathway toward degradation of environmental pharmaceutical pollutants: structure, kinetics, and mechanism approach, *Catal. Sci. Technol.*, 7 (2017) 4548–4569.
- [6] A. Zuurro, R. Lavecchia, M.M. Monaco, G. Iervolino, V. Vaiano, Photocatalytic degradation of azo dye reactive, *Catalysts*, 9 (2019) 645–661.
- [7] T. Tapia-Tlatelpa, J. Trull, L. Romeral, In situ decolorization monitoring of textile dyes for an optimized UV-LED/TiO₂ reactor, *Catalysts*, 9 (2019) 1–15.
- [8] A. Elhalil, R. Elmoubarki, M. Farnane, A. Machrouhi, F.Z. Mahjoubi, M. Sadiq, S. Qourzal, M. Abdennouri, N. Barka, Novel Ag-ZnO-La₂O₃CO₃ photocatalysts derived from the layered double hydroxide structure with excellent photocatalytic performance for the degradation of pharmaceutical compounds, *J. Sci.: Adv. Mater. Devices*, 4 (2019) 34–46.

- [9] Y.K. Mishra, R. Adelung, ZnO tetrapod materials for functional applications, *Mater. Today*, 21 (2018) 631–651.
- [10] A. Elhalil, R. Elmoubarki, M. Farnane, A. Machrouhi, M. Sadiq, F.Z. Mahjoubi, S. Qourzal, N. Barka, Photocatalytic degradation of caffeine as a model pharmaceutical pollutant on Mg-doped ZnO-Al₂O₃ heterostructure, *Environ. Nanotechnol. Monit. Manage.*, 10 (2018) 63–72.
- [11] S. Lathasree, A.N. Rao, B. Sivasankar, V. Sadasivam, K. Rengara, Heterogeneous photocatalytic mineralisation of phenols in aqueous solutions, *J. Mol. Catal. A: Chem.*, 223 (2004) 101–105.
- [12] I. Fatimah, L. Sopia, Preparation of TiO₂/MCM-41 photocatalyst using rice husk ash as silica source, *AIP Conf. Proc.*, 1823 (2017) 020124.
- [13] V.R. Batistela, L.Z. Fogaça, S.L. Fávoro, W. Caetano, N.R.C. Fernandes-Machado, N. Hioka, ZnO supported on zeolites: photocatalyst design, microporosity, and properties, *Colloids Surf., A*, 513 (2017) 20–27.
- [14] A.M. Ali, A.A. Ismail, R. Najmy, A. Al-Hajry, Preparation and characterization of ZnO-SiO₂ thin films as highly efficient photocatalyst, *J. Photochem. Photobiol., A*, 275 (2014) 37–46.
- [15] B. Hakimi, M. Ghorbanpour, A. Feizi, ZnO/bentonite nanocomposites prepared with solid-state ion exchange as photocatalysts, *J. Ultrafine Grained Nanostruct. Mater.*, 51 (2018) 139–146.
- [16] H. Mekatel, S. Amokrane, B. Bellal, M. Trari, D. Nibou, Photocatalytic reduction of Cr(VI) on nanosized Fe₂O₃ supported on natural Algerian clay: characteristics, kinetic and thermodynamic study, *Chem. Eng. J.*, 200–202 (2012) 611–618.
- [17] L. Laysandra, M.W.M.K. Sari, F.E. Soetaredjo, K. Foe, J.N. Putro, A. Kurniawan, Y.-H. Ju, S. Ismadji, Adsorption and photocatalytic performance of bentonite-titanium dioxide composites for methylene blue and rhodamine B decoloration, *Heliyon*, 3 (2017) e00488.
- [18] P.M. Aneesh, K.A. Vanaja, M.K. Jayaraj, Synthesis of ZnO nanoparticles by hydrothermal method, *Nanophotonic Mater. IV*, 6639 (2007) 66390J.
- [19] M. Akhtar, M. Ahamed, S. Kumar, M. Khan, J. Ahmad, S. Alrokayan, Zinc oxide nanoparticles selectively induce apoptosis in human cancer cells through reactive oxygen species, *Int. J. Nanomed.*, 7 (2012) 845–857.
- [20] K. Mamulová Kutlákova, J. Tokarský, P. Peikertová, Functional and eco-friendly nanocomposite kaolinite/ZnO with high photocatalytic activity, *Appl. Catal., B*, 162 (2015) 392–400.
- [21] K.T. Simfroso, R.T. Candidato, F.R. Bagsican, M.E. Jabian, M.K.G. Odarve, G.G. Paylaga, B.R.B. Sambo, R.M. Vequizo, A.C. Alguno, Growth mechanism of chemically prepared ZnO-SiO₂ nanostructures grown on glass and silicon substrates., *IOP Conf. Ser.: Mater. Sci. Eng.*, 79 (2015) 012031.
- [22] A. Subramanian, V. Visweswaran, C.S. Kumar, T. Sornakumar, Preparation and Characterisation of ZnO - SiO₂ and Bi₂O₃ - CuO nanocomposites, *Nanochem. Res.*, 3 (2018) 79–84.
- [23] I. Fatimah, Biosynthesis and characterization of ZnO nanoparticles using rice bran extract as low-cost templating agent, *J. Eng. Sci. Technol.*, 13 (2018) 409–420.
- [24] S. Anandan, Y. Ikuma, K. Niwa, An overview of semi-conductor photocatalysis: modification of TiO₂ nanomaterials, *Solid State Phenom.*, 162 (2010) 239–260.
- [25] Y.V. Meteleva, F. Roessner, G.F. Novikov, Synthesis and optical properties of zeolite-semiconductor composites-new photocatalysts, *J. Photochem. Photobiol., A*, 196 (2008) 154–158.
- [26] C. Purnawan, S. Wahyuningsih, V. Nawakusuma, Methyl violet degradation using photocatalytic and photoelectrocatalytic processes over graphite/PbTiO₃ composite, *Bull. Chem. React. Eng. Catal.*, 13 (2018) 127–135.
- [27] K. Saeed, I. Khan, T. Gul, M. Sadiq, Efficient photodegradation of methyl violet dye using TiO₂/Pt and TiO₂/Pd photocatalysts, *Appl. Water Sci.*, 7 (2017) 3841–3848.
- [28] K. Jeyasubramanian, G.S. Hikkur, R.K. Sharma, Photo-catalytic degradation of methyl violet dye using zinc oxide nano particles prepared by a novel precipitation method and its antibacterial activities, *J. Water Process Eng.*, 8 (2015) 35–44.
- [29] V.L. Chandraboss, J. Kamalakkannan, S. Prabha, S. Senthilvelan, An efficient removal of methyl violet from aqueous solution by an AC-Bi/ZnO nanocomposite material, *RSC Adv.*, 5 (2015) 25857–25869.
- [30] I.K. Punithavathy, J.P. Richard, S.J. Jeyakumar, M. Jothibas, P. Praveen, Photodegradation of methyl violet dye using ZnO nanorods, *J. Mater. Sci. - Mater. Electron.*, 28 (2017) 2494–2501.
- [31] S. Khezrianjoo, H. Revanasiddappa, Langmuir-Hinshelwood kinetic expression for the photocatalytic degradation of metanil yellow aqueous solutions by ZnO catalyst, *Chem. Sci. J.*, 2012 (2012) 85–85.
- [32] L. Djouadi, H. Khalaf, H. Boukhatem, H. Boutoumi, A. Kezzime, J.A. Santaballa, M. Canle, Degradation of aqueous ketoprofen by heterogeneous photocatalysis using Bi₂S₃/TiO₂-Montmorillonite nanocomposites under simulated solar irradiation, *Appl. Clay Sci.*, 166 (2018) 27–37.
- [33] I. Fatimah, R.Y. Pradita, A. Nurfalinda, Study on ZnO catalytic activity in salicylic acid degradation by sonophotocatalysis, (2017), doi: 10.3303/CET1756276.
- [34] I. Fatimah, Preparation of ZnO/cetyl trimethyl ammonium salt/hectorite as catalyst in alizarin red S photo-oxidation, *Asian J. Chem.*, 23 (2011) 4672–4676.
- [35] E.G. Pantohan, R.T. Candidato, R.M. Vequizo, Surface characteristics and structural properties of sol-gel prepared ZnO-SiO₂ nanocomposite powders, *IOP Conf. Ser.: Mater. Sci. Eng.*, 79 (2015) 012024.
- [36] A.H. Zyoud, T. Zorba, M. Helal, S. Zyoud, N. Qamhiya, A.R. Hajamohideen, S.H. Zyoud, H.S. Hilal, Direct sunlight-driven degradation of 2-chlorophenol catalyzed by kaolinite-supported ZnO, *Int. J. Environ. Sci. Technol.*, 16 (2019) 6267–6276.